



**HAL**  
open science

## Enhanced performances of structured oxygen electrodes for high temperature steam electrolysis

Tiphaine Ogier, Jean-Marc. Bassat, Fabrice Mauvy, Sébastien Fourcade, Jean-Claude Grenier, Karine Couturier, Julie Mougin, Marie Petitjean

► **To cite this version:**

Tiphaine Ogier, Jean-Marc. Bassat, Fabrice Mauvy, Sébastien Fourcade, Jean-Claude Grenier, et al.. Enhanced performances of structured oxygen electrodes for high temperature steam electrolysis. Fuel Cells, 2013, 13 (4), pp.536-541. 10.1002/fuce.201200201 . hal-00860497

**HAL Id: hal-00860497**

**<https://hal.science/hal-00860497>**

Submitted on 12 Jul 2022

**HAL** is a multi-disciplinary open access archive for the deposit and dissemination of scientific research documents, whether they are published or not. The documents may come from teaching and research institutions in France or abroad, or from public or private research centers.

L'archive ouverte pluridisciplinaire **HAL**, est destinée au dépôt et à la diffusion de documents scientifiques de niveau recherche, publiés ou non, émanant des établissements d'enseignement et de recherche français ou étrangers, des laboratoires publics ou privés.



# Enhanced Performances of Structured Oxygen Electrodes for High Temperature Steam Electrolysis<sup>▲</sup>

T. Ogier<sup>1</sup>, J. M. Bassat<sup>1</sup>, F. Mauvy<sup>1\*</sup>, S. Fourcade<sup>1</sup>, J. C. Grenier<sup>1</sup>, K. Couturier<sup>2</sup>, M. Petitjean<sup>2</sup>, J. Mougín<sup>2</sup>

<sup>1</sup> CNRS, Université de Bordeaux, ICMCB 87 Av. Dr Schweitzer, F-33600 Pessac Cedex, France

<sup>2</sup> CEA-Grenoble, LITEN/DTBH/LTH 17 rue des Martyrs, F-38054 Grenoble Cedex 9, France

## Abstract

The present study is focused on alternative structured oxygen electrodes for solid oxide electrolysis cells (SOEC). The  $\text{Ln}_2\text{NiO}_{4+\delta}$  (Ln = La or Pr) nickelate oxides were selected as innovative electrode materials with respect to their mixed electronic and ionic conductivity. A thin interfacial ceria-based layer was added in between the electrode and the zirconia-based electrolyte to improve mechanical and electrochemical properties and to limit the chemical reactivity. These structured cells were characterized by electrochemical impedance spectroscopy on symmetrical cells, under zero dc conditions and anodic polarization. Low polarization resistance  $R_P$  and improved anodic overpotential  $\eta_A$  versus current density curves were obtained for the  $\text{Pr}_2\text{NiO}_{4+\delta}$  electrode with  $\text{Ce}_{0.8}\text{Y}_{0.2}\text{O}_{2-\delta}$  interlayer:  $R_P$  is decreased down to

$0.06 \Omega \text{ cm}^2$  at  $800^\circ\text{C}$ , under air and zero dc conditions. Then, complete hydrogen electrode-supported cells including  $\text{Pr}_2\text{NiO}_{4+\delta}$  as oxygen electrode were electrochemically characterized. At  $800^\circ\text{C}$ , when the inlet gas composition is 90 vol.%  $\text{H}_2\text{O}$ –10 vol.%  $\text{H}_2$  at the hydrogen electrode, air being swept at the oxygen electrode, the current density determined at 1.28 V reaches  $-0.9 \text{ A cm}^{-2}$ , the corresponding steam to hydrogen conversion ratio being 58%. These results are compared to those obtained with a reference cell including the oxygen deficient perovskite  $\text{La}_{0.6}\text{Sr}_{0.4}\text{Fe}_{0.8}\text{Co}_{0.2}\text{O}_{3-\delta}$  as oxygen electrode.

**Keywords:** Barrier Layer, Hydrogen Production,  $\text{K}_2\text{NiF}_4$  Structure, Overpotential, Oxygen Electrode, SOEC, SOFC

## 1 Introduction

For economical and ecological reasons, hydrogen is considered as a potential energy vector for future. Before becoming an available alternative fuel, the main problem still to be solved is its massive production via clean processes with low or no  $\text{CO}_2$  emissions. High temperature steam electrolysis (HTSE) is one of the most promising ways to reach this target, with a high efficiency when compared to the conventional low temperature processes. It consists in splitting water molecules into hydrogen and oxygen gases using electricity and heat [1], which can be provided by renewable energy sources or nuclear power plants for example [2]. To reduce the required energy, the development of highly efficient systems is necessary. Each system component has to be optimized, in

particular the single solid oxide electrolysis cell (SOEC) where the electrochemical reactions occur. At the cell level, electrode polarizations induce large voltage losses that should be reduced to increase the total efficiency [3]. More precisely, improving the oxygen electrode performances is of crucial interest since this electrode contributes to a large extent to the cell polarization resistance. Compared to oxygen electrodes with pure electronic conduction, the use of a mixed electronic and ionic conducting (MEIC) oxygen electrodes (either as composite or as single phase) is especially relevant as such kind of materials is expected to extend the reaction zones all over the gas/electrode interface.

Most current studies reported on HTSE consider solid oxide cells containing perovskite-type oxygen electrodes as generally for SOFCs [4, 5]. The present study focuses on alter-

<sup>▲</sup> Paper presented at the 10th European SOFC Forum 2012, June 26–29, 2012 held in Lucerne, Switzerland. Organized by the European Fuel Cell Forum – [www.efcf.com](http://www.efcf.com)

[\*] Corresponding author, [mauvy@icmcb-bordeaux.cnrs.fr](mailto:mauvy@icmcb-bordeaux.cnrs.fr)

native structured oxygen electrodes. The  $\text{Ln}_2\text{NiO}_{4+\delta}$  (Ln = La or Pr) rare-earth nickelate oxides (with  $\text{K}_2\text{NiF}_4$ -type structure) have been selected as oxygen electrode materials with respect to their electrocatalytic activity. Indeed, their ability to accommodate oxygen over-stoichiometry and their MEIC properties when operating under oxidizing conditions [6] explains the strong interest in these compounds as solid oxide fuel cell (SOFC) cathode material [7]. Moreover, it appears that these materials show an extremely high flexibility for being used as oxygen electrode in very different conditions in terms of oxygen partial pressure or/and water content [8, 9]. In this way, it was reported that, under anodic polarization (HTSE conditions), this rare-earth nickelate oxide-type exhibits a lower polarization resistance than under cathodic polarization [10]. In addition, in SOFC devices, it has been shown several times that adding a thin doped ceria buffer layer with optimized microstructure, between the oxygen electrode and the zirconia-based electrolyte significantly increases the electrochemical properties of the cells [11–14].

In this work, such a ceria-based interfacial layer has been deposited to improve electrochemical interfacial properties and to limit the chemical reactivity between the electrode material and the electrolyte. In this frame, two different interfacial layers were compared. The corresponding structured electrodes were screen-printed and sintered, then characterized using electrochemical impedance spectroscopy (EIS) measurements performed on symmetrical electrolyte-supported cells, under zero dc conditions and also anodic polarization. Then, complete hydrogen electrode-supported cells, including  $\text{Pr}_2\text{NiO}_{4+\delta}$  structured oxygen electrode, were characterized in terms of electrochemical performances, in electrolysis working conditions.

## 2 Experimental

### 2.1 Powder Preparation and Cell Manufacturing

The  $\text{Ln}_2\text{NiO}_{4+\delta}$  (Ln = La or Pr) powders were prepared by the nitrate–citrate route, as previously described [8]. The powders were then ball milled to decrease the median particle size down to about 0.5  $\mu\text{m}$ . The selected interfacial materials were made of ceria doped with 20 mol.% yttrium or gadolinium, leading to the formula  $\text{Ce}_{0.8}\text{Y}_{0.2}\text{O}_{2-\delta}$  (YDC) and  $\text{Ce}_{0.8}\text{Gd}_{0.2}\text{O}_{2-\delta}$  (GDC) provided by Praxair<sup>®</sup> and Rhodia<sup>®</sup>, respectively. Both median particle sizes were about 0.2  $\mu\text{m}$ . Terpeneol-based slurries with YDC or GDC, then  $\text{Ln}_2\text{NiO}_{4+\delta}$  (Ln = La or Pr) powders were successively screen-printed on both sides of dense 8 mol.% yttria-doped zirconia (8YSZ) electrolyte pellets (about 1.2 mm thick). YDC and GDC layers were sintered in air at 1,400 and 1,350  $^{\circ}\text{C}$ , respectively for 1 h resulting in 3–5  $\mu\text{m}$  thick layers. The  $\text{Ln}_2\text{NiO}_{4+\delta}$  (Ln = La or Pr) electrodes were annealed for 1 h, in air, at 1,100  $^{\circ}\text{C}$  for  $\text{La}_2\text{NiO}_{4+\delta}$  and at

1,180  $^{\circ}\text{C}$  for  $\text{Pr}_2\text{NiO}_{4+\delta}$ . These sintering temperatures were beforehand optimized to obtain a controlled homogenous porous electrode microstructure. Figure 1 shows a typical example of the SEM micrographs of the cross-section for  $\text{La}_2\text{NiO}_{4+\delta}$ /8YSZ interface with or without YDC barrier layer.

In order to characterize the electrochemical properties of these structured electrodes on symmetrical cells, two geometries were used: (i) both electrodes cover all the electrolyte surface, in the case of impedance spectroscopy measurements performed under zero dc conditions (ii) a Pt reference electrode is set on one side of the electrolyte, the electrodes covering one-half of the electrolyte surface, for samples used for measuring the polarization curves ( $i_{\text{dc}} \neq 0$ ) [15].

Finally, to prepare complete electrolysis single cells, a  $\text{Pr}_2\text{NiO}_{4+\delta}$  electrode was screen-printed on a planar commercial hydrogen electrode-supported half-cell. The 5–10  $\mu\text{m}$  thick hydrogen electrode functional layer consists in a porous nickel and 8 mol.% yttria-doped zirconia cermet (Ni – 8YSZ) supported by a 500  $\mu\text{m}$  thick porous nickel and 3 mol.% yttria-doped zirconia cermet (Ni – 3YSZ). The electrolyte is a 3–5  $\mu\text{m}$  thick layer of 8 mol.% yttria-doped zirconia (8YSZ). The commercial half-cell comprises a relatively dense 3  $\mu\text{m}$  thick YDC interlayer deposited on the oxygen electrode side. The hydrogen electrode diameter was 50 mm and the oxygen electrode diameter was 20 mm. The  $\text{Pr}_2\text{NiO}_{4+\delta}$  electrode was sintered for 1 h, in air, at 1,180  $^{\circ}\text{C}$ .

### 2.2 Electrochemical Characterizations

#### 2.2.1 Investigations on Symmetrical Cell

In order to characterize the electrochemical properties of the  $\text{Ln}_2\text{NiO}_{4+\delta}$  (Ln = La or Pr) oxygen electrodes, EIS measurements were carried out under air, on symmetrical cells, in the temperature range 600–800  $^{\circ}\text{C}$ . Current collectors on both cell sides were gold grids (1,024 mesh  $\text{cm}^{-2}$ ). The impedance diagrams were recorded after reaching steady state, under potentiostatic control with 50 mV ac amplitude, from  $10^6$  Hz down to  $10^{-2}$  Hz, using a frequency response analyzer module Autolab FRA2, coupled with a potentiostat/galvanostat PGSTAT 302N. The complex impedance diagrams were fitted using an equivalent circuit by means of the Zview<sup>™</sup> software (Scribner Associates). The polarization

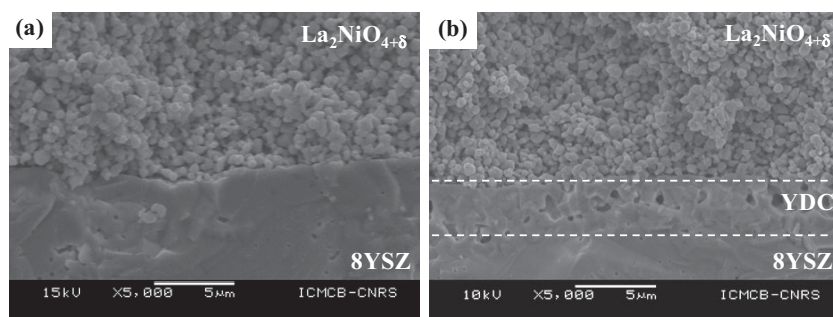


Fig. 1 Typical SEM micrographs (transverse cross-section view after fracture) for the  $\text{La}_2\text{NiO}_{4+\delta}$ /8YSZ interface (a) and the  $\text{La}_2\text{NiO}_{4+\delta}$ /YDC/8YSZ interface (b).

resistance  $R_P$  values (corresponding to the sum  $R_P = R_{HF} + R_{LF}$ ) were calculated from the difference between the low and the high frequencies diagram intercepts with the  $Z'$ -axis of the Nyquist representation.

The polarization curves were obtained by voltamperometry measurements using a three-electrode configuration, with the same apparatus and the same potentiostatic control. For each point, a constant voltage polarization  $E$  was applied between the working and the reference electrodes and the resulting current  $I$  between the working and the counter electrodes was recorded after steady state. Measurements were carried out step by step from zero dc voltage up to the highest polarization of 1 V, then back to zero dc voltage, in order to check reversibility. The impedance value obtained at the diagram  $-Z''$ -axis intercept at high frequencies, represents the series resistance  $R_S$ . The ohmic drop  $R_S I$  was deduced from the impedance diagram carried out at each investigated voltage step, which allowed determining the working electrode anodic overpotential  $\eta_A$ , according to Eq. (1):

$$\eta_A = E - R_S I \quad (1)$$

### 2.2.2 Single Cell Set-up and Measurements

The single cell characterizations were carried out using a two-atmosphere set-up (cf. Figure 2) [16]. The inlet gas composition was composed of 90 vol.%  $H_2O$ -10 vol.%  $H_2$  for the hydrogen electrode while air flew in the oxygen electrode. The area normalized flow was  $12 \text{ NmL min}^{-1} \text{ cm}^{-2}$  on the standard ambient temperature and pressure conditions, on both anode and cathode sides. The percentage of steam-to-hydrogen conversion (SC) of the SOEC during the experiments is calculated as the produced molar amount of hydrogen divided by the molar amount of water in the inlet gas. The produced hydrogen amount was calculated using the Faraday law assuming 100% current efficiency. Current collectors were gold and platinum grids for the anode, nickel grids for the cathode, in order to improve contact with the ceramic electrodes. Moreover, the current collection was optimized through the control of the compression effort. The current density  $i$  was calculated from the normalization of the recorded dc current  $I$  with respect to the geometrical oxygen electrode surface area (about  $3.14 \text{ cm}^2$ ). The polarization curves were performed under galvanostatic control, from  $0 \text{ A cm}^{-2}$  to  $-1 \text{ A cm}^{-2}$ , then back to zero current, using an Autolab PGSTAT 302N.

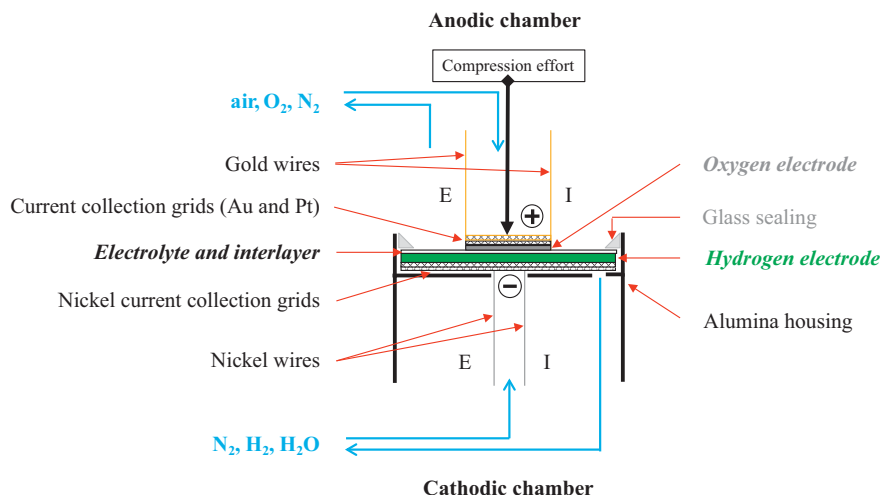


Fig. 2 Schematic representation of the experimental set-up for the single cell measurements.

## 3 Results and Discussion

### 3.1 Symmetrical Cell Characterizations

#### 3.1.1 Polarization Resistance Measurements under Air

The symmetrical cells were characterized by EIS under air. Typical diagrams measured at  $800 \text{ }^\circ\text{C}$  are shown in Figure 3 in the Nyquist representation. They are normalized by the geometrical electrode surface area (about  $1.7 \text{ cm}^2$ ) divided by two to take into account the fact that two symmetrical electrodes are surrounding the electrolyte and to obtain the electrochemical properties of one single electrode.

All the measured diagrams have been fitted using the equivalent circuit show in Figure 3, i.e. a resistance and two  $R//CPE$  elements (Constant Phase Element) associated in series. Comparing the EIS diagrams in Figure 3 underlines the significant decrease of the resistance of the high frequency

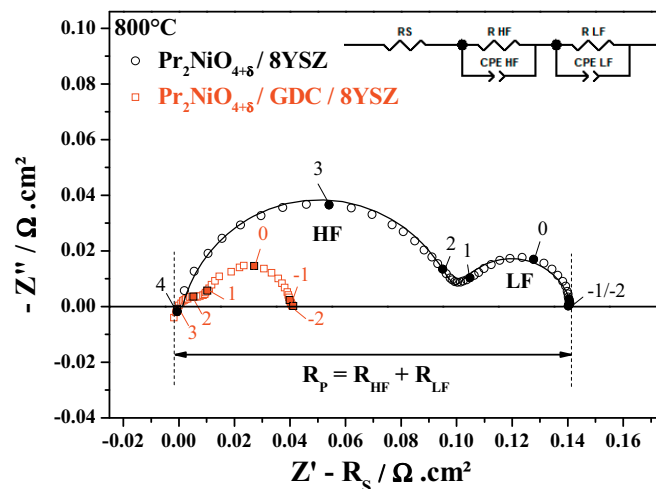


Fig. 3 Impedance diagrams recorded at  $800 \text{ }^\circ\text{C}$  under air for  $\text{Pr}_2\text{NiO}_{4+\delta}/8\text{YSZ}$  and  $\text{Pr}_2\text{NiO}_{4+\delta}/\text{GDC}/8\text{YSZ}$  symmetrical half-cells. The corresponding equivalent circuit used for fitting and the resulting simulated diagram are indicated. The numbers given on the diagrams correspond to the frequencies logarithms.

contribution  $R_{HF}$  when a GDC interlayer is present. On the contrary, the resistance of the low frequency contribution  $R_{LF}$  seems constant at 800 °C whatever the interface. The thermal evolutions of  $R_{HF}$  and  $R_{LF}$  are given in Figure 4. It can be noticed the simultaneous decrease of the high and low frequency resistances with temperature. According to previous works, the large decrease of  $R_{HF}$  can be explained by the beneficial effect of the GDC barrier layer [14]. Indeed, SEM pictures of the corresponding cells have shown that the adhesion between materials and the quality of the electrode/electrolyte interface are improved when the interlayer is present. According to the literature, the low frequency resistance  $R_{LF}$  is generally assigned to the electrode reaction processes [17, 18]. In this way,  $R_{LF}$  is supposed to be only slightly changed when adding a GDC barrier. This assumption is in good agreement with our experimental results, especially in the lowest temperature range. However, at high temperature (700–800 °C), the activation energy of  $R_{LF}$  is lower, with the value of 0.19 eV, which could indicate a modification of the reaction rate-determining step.

The polarization resistances values obtained for the structured  $\text{Ln}_2\text{NiO}_{4+\delta}$  ( $\text{Ln} = \text{La}$  or  $\text{Pr}$ ) electrodes are plotted in Figure 5.

The GDC or YDC interlayer leads to a significant decrease of the  $R_p$ , for both  $\text{La}_2\text{NiO}_{4+\delta}$  and  $\text{Pr}_2\text{NiO}_{4+\delta}$  electrodes. For instance, for  $\text{Pr}_2\text{NiO}_{4+\delta}/\text{YDC}$  half-cell, the  $R_p$  is decreased by a factor of two, down to  $0.06 \Omega \text{ cm}^2$  at 800 °C, under air and zero dc conditions. A similar value is also obtained with  $\text{Pr}_2\text{NiO}_{4+\delta}/\text{GDC}$ , at 800 °C. These values correspond to the lowest obtained  $R_p$  value in the set of data. It can be concluded that ceria-based barrier layer (and optimized sintering process and power preparation) leads to a drastic improvement of the electrode polarization resistance.

### 3.1.2 Polarization Curves

With the aim to characterize the electrochemical properties under dc current conditions, electrode polarization curves  $\eta_A = f(i)$  have been measured step by step under steady state on symmetrical cells based on  $\text{Ln}_2\text{NiO}_{4+\delta}$  ( $\text{Ln} = \text{La}$  or  $\text{Pr}$ ) materials with or without an additional GDC or YDC interfacial layer. Anodic current conditions, representative of electrolysis operation have been selected. Examples of polarization curves recorded at 800 °C, under air, are given in Figure 6.

As observed under zero dc conditions, adding a ceria-based interlayer leads to significant improvement of the polarization curves. Similar anodic overpotential  $\eta_A$  versus current density curves are obtained when a GDC or YDC interlayer is applied. Finally, because of better electrochemical properties of  $\text{Pr}_2\text{NiO}_{4+\delta}$  compared to  $\text{La}_2\text{NiO}_{4+\delta}$ , this electrode was selected for further characterizations as single electrolysis cells.

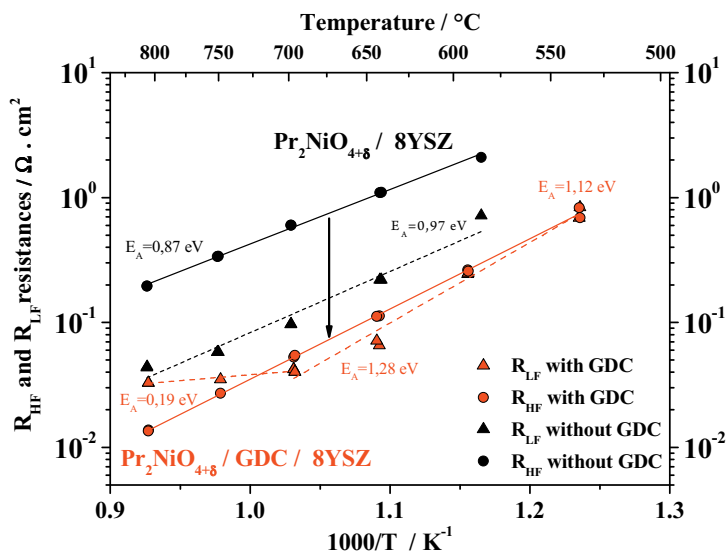


Fig. 4 Thermal variation of the resistances  $R_{HF}$  and  $R_{LF}$  measured for  $\text{Pr}_2\text{NiO}_{4+\delta}/8\text{YSZ}$  and  $\text{Pr}_2\text{NiO}_{4+\delta}/\text{GDC}/8\text{YSZ}$  symmetrical half-cells, under air. The activation energy is indicated for each resistance.

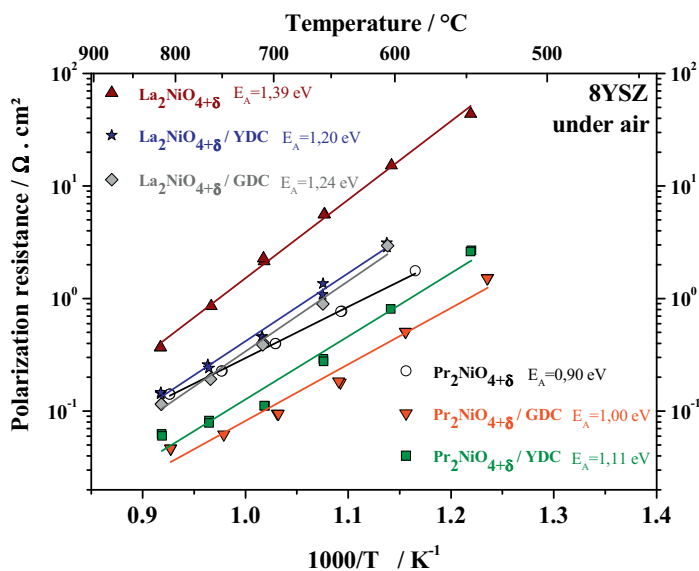


Fig. 5 Thermal variation of the polarization resistance  $R_p$  of structured electrodes measured on symmetrical cells, under air, with 8YSZ as electrolyte. The activation energy is indicated for each electrode.

### 3.2 Electrolysis Single Cell Operation

The polarization curve recorded on a single cell including  $\text{Pr}_2\text{NiO}_{4+\delta}$  oxygen electrode was compared at 800 °C to the ones obtained with two commercial hydrogen electrode-supported cells of the same type, including the – reference – oxygen deficient perovskite  $\text{La}_{0.6}\text{Sr}_{0.4}\text{Fe}_{0.8}\text{Co}_{0.2}\text{O}_{3-\delta}$ , as oxygen electrode (Figure 7). All cells had an identical YDC barrier layer. They were studied using the same experimental set-up and similar gas conditions. However, the difference observed in the polarization curves of the commercial cells likely results from disparity in their manufacture.

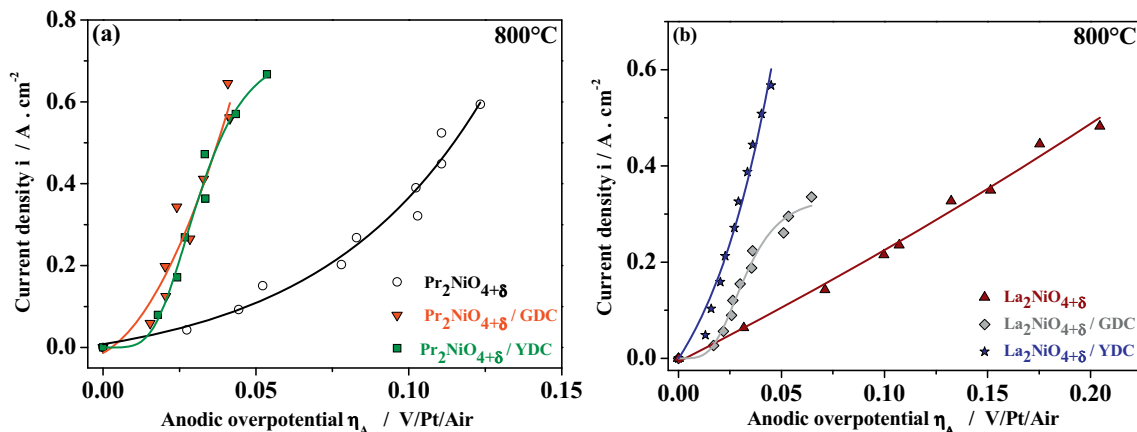


Fig. 6 Polarization curves recorded under air at 800 °C on structured symmetrical cells:  $\text{Pr}_2\text{NiO}_{4+\delta}$ ,  $\text{Pr}_2\text{NiO}_{4+\delta}/\text{GDC}$ , and  $\text{Pr}_2\text{NiO}_{4+\delta}/\text{YDC}$  (a),  $\text{La}_2\text{NiO}_{4+\delta}$ ,  $\text{La}_2\text{NiO}_{4+\delta}/\text{GDC}$ , and  $\text{La}_2\text{NiO}_{4+\delta}/\text{YDC}$  (b).

From the analysis of Figure 7, the  $i$ - $V$  curves may be divided into three parts. Firstly, the low current density range ( $i > -0.2 \text{ A cm}^{-2}$ ) is the domain where activation overvoltage dominates. In this part, the kinetics is mainly governed by the charge transfer process. The evolution of the voltage at low current densities shows that the area specific resistance (ASR) decreases as the current density increases. At the OCV, the ASR value of cell based on  $\text{Pr}_2\text{NiO}_{4+\delta}/\text{YDC}$  oxygen electrode is about  $0.71 \Omega \text{ cm}^2$  while for  $i = -0.2 \text{ A cm}^{-2}$ , the ASR is equal to  $0.40 \Omega \text{ cm}^2$ . Secondly, in the intermediate part ( $-0.6 \text{ A cm}^{-2} < i < -0.2 \text{ A cm}^{-2}$ ), the  $i$ - $V$  plot is quasi-linear. In this part, the ASR is nearly constant and minimal. This behavior is mainly assigned to the ohmic drop located in the solid electrolyte. At  $i = -0.5 \text{ A cm}^{-2}$ , the ASR is  $0.37 \Omega \text{ cm}^2$ . Finally, under high negative current densities ( $i < -0.6 \text{ A cm}^{-2}$ ), concentration overpotentials appear which

reflect the problems for the reactants to access to the active sites and the products to be evacuated from them. The kinetics is then limited by the mass transport properties. These phenomena can be divided into two processes: the diffusion of the involved species to the catalytic sites and the removal of produced hydrogen and oxygen. On the  $i$ - $V$  curve, this domain characterized by diffusion leads to an abrupt increase of the voltage and ASR when the current density increases. For  $i = -0.8 \text{ A cm}^{-2}$ , the ASR is  $0.66 \Omega \text{ cm}^2$  and for  $i = -0.9 \text{ A cm}^{-2}$  the ASR is close to  $1.20 \Omega \text{ cm}^2$ .

On the major part of the polarization curves, i.e. until  $-0.8 \text{ A cm}^{-2}$ , the studied cells show similar performances. The current density determined at thermo-neutral potential 1.28 V reaches  $-0.9 \text{ A cm}^{-2}$ , the steam conversion being about 58%.

It can be noticed that the boundaries of the three domains described for Figure 7 are valid for the experimental conditions used to obtain these data. Indeed, the borders of these

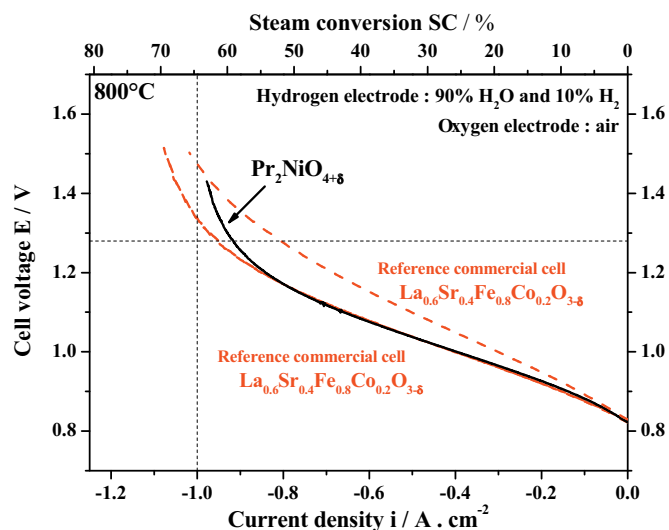


Fig. 7 Polarization curves measured on an electrolysis single cell including  $\text{Pr}_2\text{NiO}_{4+\delta}/\text{YDC}$  oxygen electrode (solid line) and two commercial cells of the same type containing  $\text{La}_{0.6}\text{Sr}_{0.4}\text{Fe}_{0.8}\text{Co}_{0.2}\text{O}_{3-\delta}/\text{YDC}$  oxygen electrode (dotted line), at 800 °C [16]. The steam-to-hydrogen conversion ratio is indicated on the secondary X-axis and the electrode gaseous conditions are also indicated.

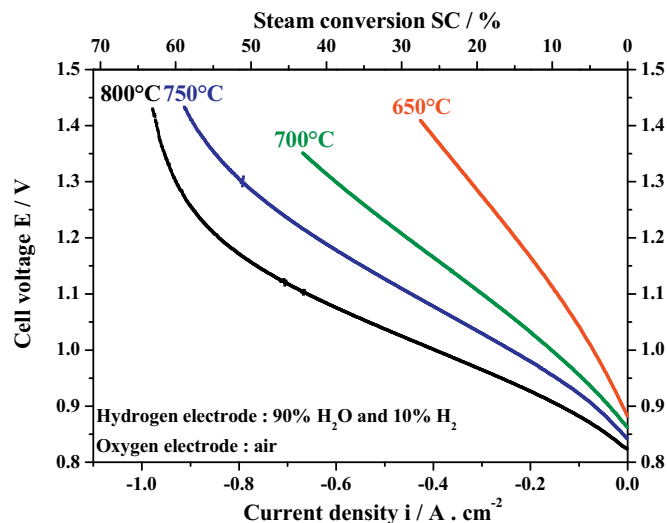


Fig. 8 Polarization curves measured on an electrolysis single cell including  $\text{Pr}_2\text{NiO}_{4+\delta}/\text{YDC}$  oxygen electrode at various temperatures. The steam conversion ratio is indicated on the secondary X-axis and the electrode gaseous conditions are also indicated.

domains depend for a given single cell on the gas flow rates and on the working temperature as shown in Figure 8 where the  $i$ - $V$  polarization curves recorded in the range 800–650 °C are reported. In particular, at 650 °C, the mass transport limitation domain is no more observable. It is due to the fact that the SC values are lower as well as the current densities in these conditions, minimizing the problems of reactant access and products evacuation to and from the active sites, respectively. The properties of the cell are mainly governed by the increase of the ohmic drop through the cell, the ASR in the linear part is 1.0  $\Omega$  cm<sup>2</sup> at 650 °C. It can be noticed that Pr<sub>2</sub>NiO<sub>4+ $\delta$</sub>  can operate as oxygen electrode down to 650 °C, leading to a promising current density close to -0.3 A cm<sup>-2</sup> for a cell voltage equals to 1.28 V.

## 4 Conclusion

MEIC materials Ln<sub>2</sub>NiO<sub>4+ $\delta$</sub>  (Ln = La or Pr) have been investigated as oxygen electrodes for HTSE. Two interfacial ceria-based layers (YDC and GDC) have been studied and both yield significant improvements. At first, the structured electrodes were characterized by EIS measurements performed on symmetrical electrolyte-supported cells, under zero dc conditions and anodic polarization. The Pr<sub>2</sub>NiO<sub>4+ $\delta$</sub> /YDC and Pr<sub>2</sub>NiO<sub>4+ $\delta$</sub> /GDC structured electrodes lead to enhanced electrochemical properties compared to the electrode without any interlayer.

Then, a complete hydrogen electrode supported cell, including the Pr<sub>2</sub>NiO<sub>4+ $\delta$</sub> /YDC structured oxygen electrode, was characterized in terms of electrochemical performances and compared to reference cells including the oxygen deficient perovskite La<sub>0.6</sub>Sr<sub>0.4</sub>Fe<sub>0.8</sub>Co<sub>0.2</sub>O<sub>3- $\delta$</sub>  as oxygen electrode and the same YDC interlayer. At 800 °C, when the inlet gas composition is 90% H<sub>2</sub>O–10% H<sub>2</sub> at the hydrogen electrode, and flowing air at the oxygen electrode, the current density reaches -0.9 A cm<sup>-2</sup> at 1.28 V, the steam to hydrogen conversion ratio being 58%. One can consider that this alternative cell shows similar performances than the commercial cells. According to these promising results, the Ln<sub>2</sub>NiO<sub>4+ $\delta$</sub>  (Ln = La or Pr) nickelates associated with a ceria-based interlayer can be considered as good candidates for oxygen electrode materials of HTSE cells. However, long-term durability should be studied for both kinds of cells; the tests are in progress.

## 5 Acknowledgments

Authors gratefully acknowledge the French Research National Agency (ANR) through “H2 and Fuel Cells program” (project FIDELHYO n°ANR-09-HPAC-005) for supporting parts of this work. We also thank Benoit Sommacal for technical assistance on electrochemical experiments.

## 6 References

- [1] W. Dönitz, E. Erdle, R. Streicher, *Electrochemical Hydrogen Technologies. Electrochemical Production and Combustion of Hydrogen*, H Wendt, New York, USA, **1990**, pp. 213.
- [2] R. Elder, R. Allen, *Prog. Nucl. Energy* **2009**, *51*, 500.
- [3] E. Ivers-Tiffée, A. V. Virkar, *High Temperature Solid Oxide Fuel Cells. Fundamentals, Design and Applications*, Elsevier, Oxford, United Kingdom, **2003**, pp. 229.
- [4] J. S. Herring, J. E. O'Brien, C. M. Stoots, G. Hawkes, J. J. Hartvigsen, M. Shahnam, *Int. J. Hydrogen Energy* **2007**, *32*, 440.
- [5] A. Brisse, J. Schefold, M. Zahid, *Int. J. Hydrogen Energy* **2008**, *33*, 5375.
- [6] E. Boehm, J. M. Bassat, P. Dordor, F. Mauvy, J. C. Grenier, P. Stevens, *Solid State Ionics* **2005**, *176*, 2717.
- [7] H. Zhao, F. Mauvy, C. Lalanne, J. M. Bassat, S. Fourcade, J. C. Grenier, *Solid State Ionics* **2008**, *179*, 2000.
- [8] J. C. Grenier, F. Mauvy, C. Lalanne, J.-M. Bassat, F. Chauveau, J. Mougín, J. Dailly, M. Marrony, *ECS Trans.* **2009**, *25*, 2537.
- [9] M. A. Laguna-Bercero, N. Kinadjan, R. Sayers, H. El Shinnawi, C. Greaves, S. J. Skinner, *Fuel Cells* **2011**, *11*, 102.
- [10] D. Pérez-Coll, A. Aguadero, M. Escudero, L. Daza, *J. Power Sources* **2009**, *192*, 2.
- [11] A. Mai, V. A. Haanappel, F. Tietz, D. Stöver, *Solid State Ionics* **2006**, *177*, 2103.
- [12] N. Jordan, W. Assenmacher, S. Uhlenbruck, V. Haanappel, H. Buchkremer, D. Stöver, W. Mader, *Solid State Ionics* **2008**, *179*, 919.
- [13] F. P. van Berkel, Y. Zhang-Steenwinkel, G. Schoemakers, M. van Tuel, B. G. Rietveld, *ECS Trans.* **2009**, *25*, 2717.
- [14] C. Ferchaud, J. C. Grenier, Y. Zhang-Steenwinkel, M. M. van Tuel, F. P. van Berkel, J. M. Bassat, *J. Power Sources* **2011**, *196*, 1872.
- [15] T. Ogier, F. Chauveau, J. M. Bassat, F. Mauvy, J. C. Grenier, J. Mougín, M. Petitjean, *ECS Trans.* **2011**, *35*, 1817.
- [16] A. Mansuy, J. Mougín, M. Petitjean, F. Mauvy, *10th European Solid Oxide Fuel Cell Forum 2012*, Luzern, Switzerland, **2012**.
- [17] F. Mauvy, C. Lalanne, J. M. Bassat, J. C. Grenier, H. Zhao, L. Huo, P. Stevens, *J. Electrochem. Soc.* **2006**, *153*, A1547.
- [18] C. Lalanne, G. Prosperi, J. M. Bassat, F. Mauvy, S. Fourcade, P. Stevens, M. Zahid, S. Diethelm, J. Van herle, J. C. Grenier, *J. Power Sources* **2008**, *185*, 1218.